



ETH zürich

INTERANNUAL VARIATIONS IN TROPICAL PACIFIC OCEAN HEAT UPTAKE AND REDISTRIBUTION

Proposal for
Master Thesis in Atmospheric and Climate Science
by
Maurice Huguenin-Virchaux
at the Climate Change Research Centre, UNSW Sydney

Supervisors:

Prof. Dr. Reto Knutti - reto.knutti@env.ethz.ch (ETH Zurich)
Dr. Iselin Medhaug - iselin.medhaug@env.ethz.ch (ETH Zurich)
Prof. Dr. Matthew H. England - m.england@unsw.edu.au (UNSW Sydney)
Dr. Ryan Holmes - ryan.holmes@unsw.edu.au (UNSW Sydney)

30th June 2017

Abstract

The El Niño-Southern Oscillation (ENSO) climate phenomenon consisting of the two phases El Niño and La Niña is the most pronounced variation of the Earth's climate system on the interannual time scale. El Niño and La Niña events are driven by strong positive feedbacks of both the atmosphere and ocean and, among others, impact the global distribution of carbon dioxide and heat. As the ocean takes up a major part of the additional anthropogenic-induced heat in the climate system, it is of importance to gain further insight into how the ENSO governs ocean heat content (OHC) anomalies. This thesis using the global ocean-sea ice model GFDL-MOM025 will quantify global and regional interannual heat uptake and redistribution caused by various events. Time-varying El Niño and La Niña-related atmospheric anomaly fields from the ERA-Interim reanalysis product are derived from an Empirical Orthogonal Function analysis of tropical Pacific wind stress anomalies and added to the model's own equilibrated forcing. Isolated anomalies make it possible to simulate semi-permanent sequestration of ocean heat throughout different scenarios including strong, moderate and consecutive El Niño and La Niña events. Comparisons between model runs will reveal how these ocean heat content anomalies depend on the non-linearities associated with ENSO and whether they can result in irreversible changes in OHC that could potentially persist for longer time periods. In contrast to a previous observation-based study using ocean buoy data for the time period 2004–2014, the model simulations used here enable to analyse OHC anomalies not only during moderate but also over the course of particular strong events. Evaluating the role of ocean heat during and also after strong events such as the 1997/1998 El Niño and may thus provide valuable insight into the governing dynamics of the ENSO.

Contents

Abstract	i
1 Introduction	1
2 Objectives	4
3 Data and Methods	5
3.1 The Ocean–Sea Ice Model	5
3.2 Experimental Design	6
3.2.1 EOF Analysis of Wind Stress Anomalies	8
3.2.2 Heat Calculation	11
4 Timeline	12
Bibliography	13

Introduction

The El Niño–Southern Oscillation (ENSO) in the equatorial Pacific Ocean consists of the two main phases El Niño and La Niña. They both have profound impacts on sea surface temperature (SST), wind stress anomalies and ocean heat content (OHC), especially in the upper few hundred meters of the tropical Pacific Ocean (Jin, 1997; Roemmich and Gilson, 2011; Lengaigne et al., 2012). Observational ocean buoy data from the Argo program illustrate large-scale heat uptake and redistribution during El Niño and La Niña events with influence on the global average (Johnson and Birnbaum, 2017).

To determine the two phases of the oscillation, the oceanic Niño index (ONI) is commonly used. According to the National Oceanographic and Atmospheric Administration’s Climate Prediction Center (2017), the ONI is defined as a 3-month running mean SST departure in the Niño3.4 region (5°S – 5°N and 170°W – 120°W) based on a 30-year climatological period (see Figure 1.1). In this study, the climatological period 1979–2016 is used. An El Niño (La Niña) event with this index is classified as a departure of greater or equal to $+0.5^{\circ}\text{C}$ (-0.5°C) for at least five consecutive overlapping 3-month seasons.

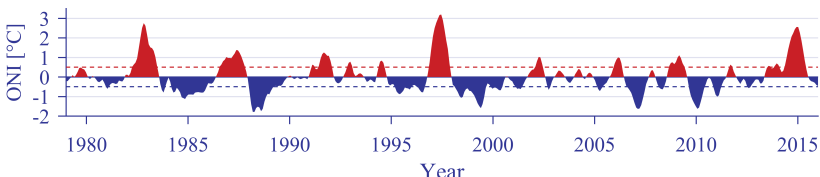


Figure 1.1: Time evolution of the ONI for 1979–2016 using SST data from the ECMWF Era-Interim product (Dee et al., 2011). Positive anomalies are shown in red and negative anomalies in blue. The red (blue) dashed horizontal line indicates the threshold of $+0.5^{\circ}\text{C}$ (-0.5°C) which has to be exceeded for an event to be classified as an El Niño (La Niña).

El Niño builds as trade winds weaken, leading to warm water masses shifting from west to east (Meinen and McPhaden, 2000). The tropical Pa-

cific starts to accumulate heat predominantly in the surface layer 0–120 m in a zonally elongated pattern around the equator while cooling dominates in the subsurface layer between 120–440 m of the western tropical Pacific (Johnson and Birnbaum, 2017). El Niño variability in surface layer heat content is thus partially cancelled by that in the subsurface layer (Roemmich and Gilson, 2011). Both diabatic (i.e. vertical mixing and heating of water masses by the solar penetrative flux) and adiabatic processes (i.e. meridional transport) play an important role in the build-up of increased warm water volume (WWV) prior to an El Niño event (Lengaigne et al., 2012).

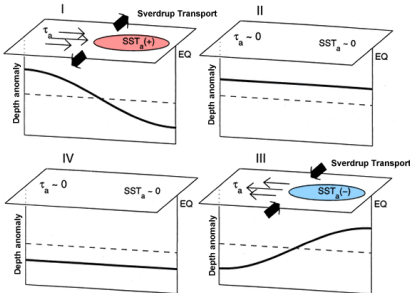


Figure 1.2: Idealized schematic of the ENSO oscillation from Meinen and McPhaden (2000). “All shown quantities are anomalies relative to the climatological mean. The bold line represents the depth anomaly of the thermocline separating warm surface water from colder deep water masses. τ_a and SST_a denote wind stress and sea surface temperature anomalies. The bold arrows show meridionally diverging and converging Sverdrup transport as a result of wind stress anomalies and the Coriolis force. An oscillation acting on a 2–7 year time scale follows the panel numbering clockwise with panel I representing El Niño and panel III representing La Niña conditions” (Meinen and McPhaden, 2000).

The reduced trade wind strength in combination with the shift in WWV to the eastern Pacific lead to a decrease in upwelling of cold water masses there (McPhaden et al. (2006), see panel I in Figure 1.2). The deepening of the thermocline excites equatorially trapped eastward (westward) travelling Kelvin (Rossby) waves with a group speed of ~ 2.8 (~ 0.9) $m s^{-1}$ (Wang et al., 2016). These two interior ocean wave types are important in propagating the anomalous signals throughout the Pacific Ocean (Stewart, 2008). At the peak of the El Niño event, most of the previously accumulated heat is released into the atmosphere resulting in increased atmospheric temperatures. Satellite-based estimates suggest a $1^\circ C$ increase in equatorial Pacific SST (indicating an El Niño event) corresponds to an increase of $3.4 \cdot 10^{21} J$ in the atmosphere (Johnson and Birnbaum, 2017).

As the ocean continuously releases heat during the event, subsurface layers cool and the thermocline shallows to positive depth anomalies (panel II in Figure 1.2). Due to the delayed nature of this proposed oscillation mechanism by Jin (1997), anomalies returning to neutral conditions tend to tip into their respective other phase and further intensify as a result

of positive feedbacks (Burgers et al., 2005). The end of an El Niño event usually coincides with the meeting of Kelvin and Rossby waves after they are reflected at the eastern and western boundary of the tropical Pacific basin. On average, it takes one year for the waves excited at the start of an El Niño to travel across the Pacific, to be reflected at the boundaries and to meet again (Stewart, 2008).

When trade winds return to their normal strength (as indicated by $\tau_a \sim 0$ in panel III), upwelling slowly resumes at the eastern boundary of the tropical Pacific. Cold water masses reach the surface and reduce local SST values. The east-west surface ocean temperature contrast amplifies the trade winds since atmospheric surface pressure above cold water is higher than over warm water masses resulting in a positive feedback (McPhaden, 2015).

During La Niña events with stronger than average easterly trade winds, cool SST values are enhanced (panel III in Figure 1.2). The accelerated trade winds intensify equatorial upwelling of cold water masses which take up large amounts of excess heat from the atmosphere (Meehl et al., 2011; Roemmich and Gilson, 2011). This heat is primarily stored in the mid-depth layers of the western Pacific as these water masses flow adiabatically along density surfaces into the ocean's interior and once again increase the WWV (Lengaigne et al., 2012).

Panel IV shows equatorial Pacific surface anomalies again at neutral state with a negative thermocline anomaly as the WWV is at its maximum. This is a direct result of large-scale heat uptake during the preceding La Niña event. The additional accumulated heat will be released into the atmosphere during the next El Niño event.

This simplified oscillation assumes that all accumulated anomalous heat during neutral states and La Niña events is being released again during El Niño events. However, Lengaigne et al. (2012) propose that also non-linear mechanisms drive both heat uptake and redistribution. These perturbations in diabatic mixing could result in the sequestration of heat into deeper, cooler layers and lead to irreversible changes in OHC that could potentially persist for longer time periods. In contrast, adiabatic rearrangement of heat (for instance by transport through the boundary currents into higher latitudes) is more easily reversible if the wind stresses return to their original values (Lengaigne et al., 2012). Warming of deep ocean layers by diabatic mixing would directly result in thermosteric sea level rise and with the current rate of climate change threaten the existence of small Pacific island states (Nurse et al., 2013).

Objectives

The Argo record operational since the early 2000 and analysed for the time period 2004–2014 in the study by [Johnson and Birnbaum \(2017\)](#) shows OHC anomalies during moderate ENSO oscillations. Particular strong El Niños such as the 1997/1998 event and their heat anomalies are not yet discussed. With the help of ocean sea-ice models, it is possible to also quantify how particular strong El Niño and La Niña events regulate OHC while ignoring all other major interannual anomalies in the Earth’s climate system. Identifying regions of heat uptake and loss during these strong events in this thesis will give valuable insight into what can be expected in regards to climate change. Therefore, this thesis can set the stage for further research on the effects of warmer tropical Pacific waters on the carbon cycle and sea level rise. The evaluation of the individual model simulations will include two steps. The first one involves the preparation of anomalous atmospheric forcing fields to simulate idealized El Niño and La Niña events in a climate model and the second one being the analysis of OHC anomalies for each simulation.

The steps involving the model simulations include:

- Performing an Empirical Orthogonal Function (EOF) analysis of wind stress anomalies in the equatorial Pacific region will result in two principle component (PC) time series closely related to the ONI.
- Creating idealized atmospheric anomaly fields with these time series to obtain symmetric El Niño and La Niña events.
- Adding these anomaly fields onto an equilibrated climate model run with no other sources of major interannual variability to simulate events.

Heat budgets will be calculated with the following goals in mind:

- Quantifying global average and regional OHC anomalies after each model simulation to identify regions of heat uptake and loss.
- Evaluating the role of the ocean circulation and the Indonesian Through-flow in heat uptake and transport.
- Evaluating how anomalies depend on the non-linearities associated with ENSO, namely the asymmetry and amplitude of the events, and whether they can result in irreversible changes in OHC that could persist for longer time periods.

3

Data and Methods

3.1 The Ocean–Sea Ice Model

The model this study will use is the GFDL-MOM025 global ocean and sea-ice model based on the Geophysical Fluid Dynamics Laboratory CM2.5 coupled climate model ([Delworth et al., 2012](#)). The model’s grid cell resolution is $1/4^\circ$ with 50 vertical depth levels ([Delworth et al., 2012](#)). Its atmospheric state is prescribed by eight fields (see Table 3.1) and converted to ocean surface fluxes using bulk formulae ([Spence et al., 2014](#)). These surface fluxes are zonal and meridional wind stress, surface heat and freshwater fluxes.

Prior to this study, the model was run for a 550-year period with CORE normal year forcing (CNYF) to equilibrium ([Large and Yeager, 2004](#)). Repeated annual cycles of the CNYF are applied to obtain a climatological average state, characterized by neutral ENSO conditions and neutral states of other climate modes ([Large and Yeager, 2004; Maher, 2016](#)).

Most climate models including the one being used in this study experience long-term changes without external influence ([Spence et al., 2014](#)). This is referred to as ‘drift’ and can influence results, especially in the deep ocean ([Maher, 2016](#)). Concluding from the study by [Maher \(2016\)](#), it is expected that the model drift will only constitute a minor error but even so will be removed from all calculations. Thereby, for all experiments in this study, a parallel control simulation that starts with identical initial conditions and is only subject to CNYF is run and subtracted from each experiment ([Maher, 2016](#)).

3.2 Experimental Design

To evaluate the impact of the ENSO on the model's heat storage, idealized forcing fields are added on top of CNYF fields. Twelve individual model experiments will be run. Each model run will vary in the added forcing anomaly fields and will span the time period of the particular event (about one year). The additional atmospheric forcing anomalies are based on the first two leading EOF modes of wind stress variability in the tropical Pacific. The PC time series of these modes are required to obtain the temporal evolution of all anomaly fields in a similar fashion. Each of the model simulations which will be conducted in this study are listed below.

- EXP₁: simulation of a strong El Niño event consisting of a combination of the three strongest observed events from 1979–2016. Hereby, the temporal evolution of the anomaly fields is a composite of the PC time series of the three events
- EXP₂: moderate El Niño event with a Niño3.4 value of +1°C which allows a comparison with the study conducted by ([Roemmich and Gilson, 2011](#)) based on ocean buoy data
- EXP₃: strong La Niña event consisting of a combination of the three strongest observed events from 1979–2016
- EXP₄: moderate La Niña event with a Niño3.4 value of -1°C
- EXP₅: full ENSO cycle consisting of both EXP₃ and EXP₁ in succession
- EXP₆: same experiment as EXP₅ but with El Niño first and La Niña second to examine whether the order of events matters
- EXP_{7–12}: this set of experiments will apply the anomalous forcing of EXP_{1–6} only over the Pacific Ocean basin (40°S–40°N) instead of the full globe to separate changes in the Pacific from changes in the other regions. For instance, Indian Ocean Dipole events (i.e. IOD⁺ with cooler (warmer) than normal eastern (western) Indian Ocean SST) often co-occur with an El Niño and influence its OHC anomalies

The atmospheric fields for each experiment are based on the interim European Centre for Medium-Range Weather Forecasts (ECMWF) Re-Analysis (ERA-Interim) product ([Dee et al., 2011](#)). These datasets are downloaded for the time period 1979–2016 and listed in the following table.

Symbol	Unit	Description
u_{10}	[m s ⁻¹]	Zonal wind at 10 m
v_{10}	[m s ⁻¹]	Meridional wind at 10 m
T_{10}	[K]	Air temperature at 10 m ¹
$q_{v,10}$	[kg kg ⁻¹]	Specific humidity at 10 m
F_{LW}^{\downarrow}	[W m ⁻²]	Downward long-wave radiative flux at the surface
F_{SW}^{\downarrow}	[W m ⁻²]	Downward short-wave radiative flux at the surface
R	[mm]	Precipitation or rain rate at the surface
SLP	[Pa]	Sea level pressure ^{1,2}
Additional Fields		
$T_{d,10}$	[K]	Dew point temperature at 10 m ^{1,2}
SST	[K]	Sea surface temperature ³
SSS	[g kg ⁻¹]	Sea surface salinity ⁴

Table 3.1: The eight atmospheric fields from the ERA-Interim product used for calculating zonal and meridional wind stress, surface heat and freshwater fluxes to force the GFDL-MOM025 model. Additional fields in the lower section are used for derivation of input fields or further calculations. All fields are downloaded on a 3/4° grid and later adjusted to the model's grid cell resolution.

¹ Air and dew point temperatures as well as pressure in the ERA-Interim product are only available on 2 m and sea surface respectively. It is assumed that using these fields rather than fields at 10 m results in a negligible difference.

² Fields required for the calculation of specific humidity

$$q_v := \frac{0.622 \cdot e}{(SLP \cdot 10^{-2}) - (0.378 \cdot e)} \mid e = 6.112 \cdot e^{\left(\frac{17.67 \cdot (T_d - 273.15)}{(T_d - 273.15) + 143.5}\right)}, \text{ Bolton (1980).}$$

³ Used to determine ENSO phases by calculating the Niño3.4 index.

⁴ Required as a restoring variable to keep the model salinity from drifting. This field is obtained from the ECMWF Ocean Re-Analysis (ORAS4) product (Balmaseda et al., 2013; Mogensen et al., 2012).

Figure 3.1 illustrates the atmospheric anomaly fields at a specific time during an El Niño event. Anomalies are generally restricted to the Pacific Ocean but also influence the global scale. During each experiment, the anomaly fields shown here will vary in extent and amplitude with time and serve as the basis to construct the idealized ENSO events. These figures here are derived from the first two principle components of an EOF analysis of equatorial Pacific wind stress anomalies which will be discussed in more detail in the next section.

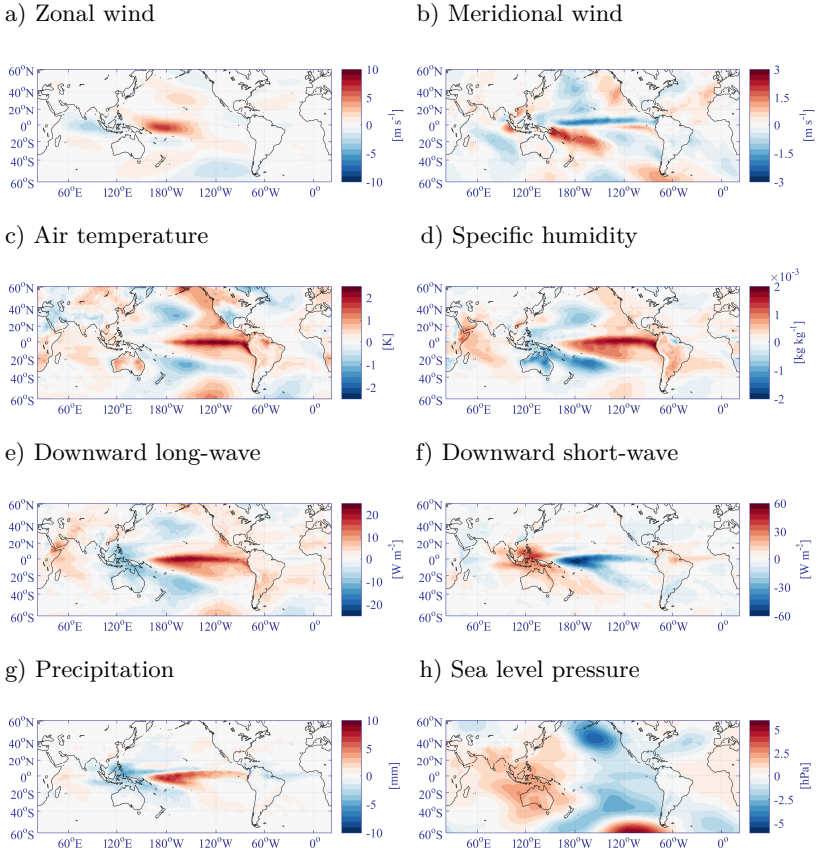


Figure 3.1: ENSO-related regression patterns of the eight atmospheric anomaly fields specified in Table 3.1 for the time period 1979–2016.

3.2.1 EOF Analysis of Wind Stress Anomalies

To construct idealized ENSO forcing fields from these datasets, an EOF analysis is used. This procedure results in spatial patterns of variability (i.e. **EOF₁**, **EOF₂**, etc.) and their associated principle components or amplitudes over time (defined as PC_1 , PC_2 , etc.). It allows to simplify the forcing into a compact set of modes and extract the most useful information that isolates only the ENSO. As shown in McGregor et al. (2014), the first two EOF patterns and their PC time series of wind stress anomalies over the tropical Pacific region (10°N – 10°S and 100°E – 60°W) are related to the ENSO.

Calculation of Wind Stress Anomalies

Monthly mean wind stress anomalies from the ERA-Interim's zonal and meridional wind speeds after detrending and removing the seasonal signal based on a 1979–2016 climatology are calculated by

$$\boldsymbol{\tau}_{10}(t) = (\boldsymbol{\tau}_{x,10}(t), \boldsymbol{\tau}_{y,10}(t)) = \rho_a \cdot C_D \cdot |\mathbf{U}(t)| \cdot (\mathbf{u}_{10}(t), \mathbf{v}_{10}(t)) \quad (3.1)$$

where $\boldsymbol{\tau}_{10}(t)$ [N m^{-2}] is the time dependent wind stress field at 10 m height consisting of zonal (i.e. west–east, $\boldsymbol{\tau}_x$) and meridional (i.e. north–south, $\boldsymbol{\tau}_y$) components, ρ_a is the density of air (1.25 kg m^{-3}), C_D is the unitless non-linear drag coefficient based on [Large and Pond \(1981\)](#) modified for low wind speeds ([Trenberth et al., 1990](#)), $|\mathbf{U}| = \mathbf{U}(\mathbf{u}_{10}, \mathbf{v}_{10})$ is the magnitude of wind speed as a function of zonal and meridional wind and \mathbf{u}_{10} and \mathbf{v}_{10} are the wind speeds in [m s^{-1}].

EOF Decomposition

An EOF analysis includes two steps: First the computation of the covariance matrix $\boldsymbol{\Sigma}$ as displayed in equation 3.2. $\boldsymbol{\Sigma}$ contains key patterns of variation within the wind stress anomaly dataset. As a second step, the solution to the eigenvalue problem in Equation 3.3 is calculated.

$$\boldsymbol{\Sigma} = \text{var}(\boldsymbol{\tau}_{10}) = \frac{1}{N-1} \cdot \boldsymbol{\tau}_{10}^T(t) \cdot \boldsymbol{\tau}_{10}(t) \quad t = 1, \dots, N \quad (3.2)$$

$$\boldsymbol{\Sigma} \cdot \mathbf{EOF}_i = PC_i(t) \cdot \mathbf{EOF}_i \quad i = 1, \dots, k \quad (3.3)$$

where N is the temporal length of the dataset, $\boldsymbol{\tau}_{10}^T(t)$ is the transposed wind stress anomaly field dependent on time, \mathbf{EOF}_i is the i -th pattern, PC_i its associated amplitude and k is the number of principle components.

The resulting first two patterns and amplitudes can be viewed in Figure 3.2. \mathbf{EOF}_1 features the equatorially symmetric anomalous Walker circulation during an El Niño event. It is characterized by westerly wind anomalies in the western tropical Pacific (see Figure 3.2a). PC_1 , the associated time series, is well correlated with monthly Niño3.4 SST anomalies ($r = 0.748$), the ONI ($r = 0.770$) and consistent with the study by [McGregor et al. \(2014\)](#). \mathbf{EOF}_2 with a strong meridional (i.e. north–south) shear of zonal wind across the Equator and a southward-shifted westerly wind anomaly plays an important role in terminating an El Niño event when this mode changes sign ([Stuecker et al., 2015](#)).

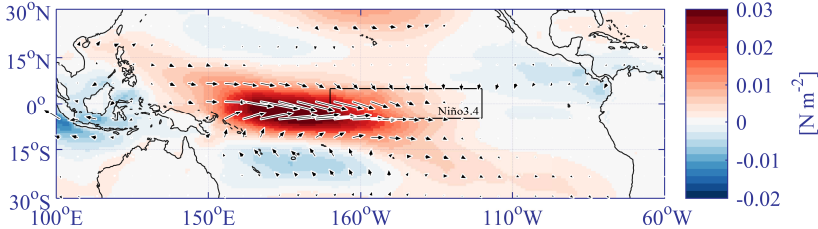
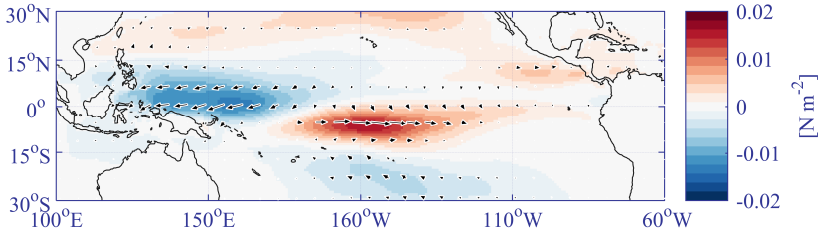
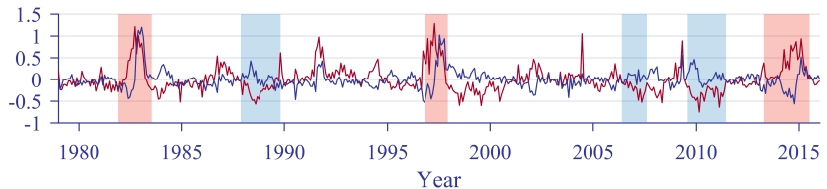
a) EOF_1 (58.6% variance)b) EOF_2 (28.9% variance)c) PC_1 and PC_2 time series

Figure 3.2: In a) and b) wind stress patterns related to El Niño and La Niña showing the first and second mode of the EOF analysis. The zonal wind stress component is shaded. In c) the associated time series of the principal components with PC_1 in red and PC_2 in blue. Red (blue) shaded areas indicate the duration of the three strongest El Niño (La Niña) events. The Niño3.4 area (5°S – 5°N and 170°W – 120°W) is indicated as the framed area in a).

Only the first two modes are used to obtain the idealized temporal evolution of the anomaly fields as these explain a large percentage (87.5%) of the wind stress variance in this region. Using these modes is also consistent with previous studies by McGregor et al. (2013, 2014). Each anomaly field at a certain stage during a synthetic ENSO oscillation can conveniently be

reconstructed with the first two *PCs* by

$$\mathbf{X}_{ideal.}(t) = \sum_{t=1}^2 PC_i(t) \cdot \mathbf{X}(t) \quad (3.4)$$

where $\mathbf{X}_{ideal.}(t)$ is one of the eight idealized forcing anomaly fields dependent on time and \mathbf{X} is the original anomaly field. The advantage with this procedure is that all anomaly fields behave in a similar manner throughout the events.

3.2.2 Heat Calculation

Simulating idealized El Niño and La Niña events with no other sources of major interannual variability allows an evaluation of the ENSO cycles influence on ocean heat uptake and redistribution. In this study, OHC anomalies in each model grid cell relative to the control simulation are calculated as

$$OHC(t) = \rho_0 \cdot c_p \cdot \int \int \int (\Theta(t) - \Theta_r(t)) dx dy dz \quad (3.5)$$

where ρ_0 is the reference density of sea water (1035 kg m^{-3}), c_p is the specific heat capacity of sea water at constant pressure ($3.992 \text{ J kg}^{-1} \text{ K}^{-1}$), $\Theta = \Theta(S_A, T, p_0, t)$ is the conservative temperature [K] as a function of absolute Salinity S_A [g kg^{-1}], sea water temperature T [$^\circ\text{C}$], sea surface pressure p_0 (101325 Pa) and time t . Θ_r is the reference conservative temperature taken from an unforced CNYF control simulation and is a function of space and time. Absolute salinity and conservative temperature will be calculated using the Thermodynamic Equation of Seawater 2010 (TEOS-10) toolbox ([Intergovernmental Oceanographic Commission, 2010](#)).

By calculating the simulated heat content anomalies as a result of several idealized El Niño and La Niña events, this thesis allows to identify the underlying physical processes that govern uptake and distribution of energy on the interannual time scale. It is expected that diabatic mixing transports warm water masses into deeper and cooler layers of the tropical Pacific Ocean. The resulting thermal expansion of these layers would lead to sea level rise and in the context of current climate change with its increased atmospheric heat signals could very well be the death penalty for small Pacific island states.

4

Timeline

06. 05. 2017	Completion of UNSW enrolment.
23. 05. 2017	Submission of Proposal.
20. 06. 2017	Proposal reviews back.
30. 06. 2017	Resubmission of revisions.
22. 08. 2017 – 14. 09. 2017	Organization of server access UNSW and moving of datasets.
11. 09. 2017 – 25. 09. 2017	Flight to Sydney and organization of long-term accommodation.
25. 09. 2017	Start Master Thesis.
25. 09. 2017 – 07. 10. 2017	Completion of EOF Analysis as in McGregor et al. (2014) with $PC_1 =$ NOAA's ERSST v4 Niño3.4.
15. 11. 2017	Completion of EXP ₁ model run.
15. 11. 2017 – 30. 11. 2017	Presentation of Seminar II.
22. 12. 2017	Completion of remaining model runs.
23. 12. 2017 – 07. 01. 2018	Christmas Holiday break.
08. 01. 2018 – 08. 03. 2018	Writing and review period.
08. 03. 2018	Finish full first draft.
08. 04. 2018	End Master Thesis.

Bibliography

- Balmaseda, M. A., Mogensen, K., and Weaver, A. T. Evaluation of the ECMWF ocean reanalysis system ORAS4. *Quarterly Journal of the Royal Meteorological Society*, 139(674):1132–1161, 2013.
- Bolton, D. The Computation of Equivalent Potential Temperature. *Monthly Weather Review*, 108(7):1046–1053, 1980.
- Burgers, G., Jin, F.-F., and Van Oldenborgh, G. J. The simplest ENSO recharge oscillator. *Geophysical Research Letters*, 32(13), 2005.
- Dee, D., Uppala, S., Simmons, A., Berrisford, P., Poli, P., Kobayashi, S., Andrae, U., Balmaseda, M., Balsamo, G., Bauer, P., et al. The ERA-Interim reanalysis: Configuration and performance of the data assimilation system. *Quarterly Journal of the Royal Meteorological Society*, 137(656):553–597, 2011.
- Delworth, T. L., Rosati, A., Anderson, W., Adcroft, A. J., Balaji, V., Benson, R., Dixon, K., Griffies, S. M., Lee, H.-C., Pacanowski, R. C., et al. Simulated Climate and Climate Change in the GFDL CM2.5 High-Resolution Coupled Climate Model. *Journal of Climate*, 25(8):2755–2781, 2012.
- Intergovernmental Oceanographic Commission. The international thermodynamic equation of seawater–2010: Calculation and use of thermodynamic properties. *Manuals Guide*, 56:196, 2010.
- Jin, F.-F. An equatorial ocean recharge paradigm for ENSO. Part I: Conceptual model. *Journal of the Atmospheric Sciences*, 54(7):811–829, 1997.
- Johnson, G. C. and Birnbaum, A. N. As El Niño builds, Pacific Warm Pool expands, ocean gains more heat. *Geophysical Research Letters*, 44(1):438–445, 2017.
- Large, W. and Pond, S. Open Ocean Momentum Flux Measurements in Moderate to Strong Winds. *Journal of Physical Oceanography*, 11(3):324–336, 1981.
- Large, W. G. and Yeager, S. G. Diurnal to Decadal Global Forcing for Ocean and Sea-Ice Models: The Data Sets and Flux Climatologies. *NCAR Technical Note*, 2004.
- Lengaigne, M., Hausmann, U., Madec, G., Menkès, C., Vialard, J., and Molines, J.-M. Mechanisms controlling warm water volume interannual

- variations in the equatorial Pacific: Diabatic versus adiabatic processes. *Climate Dynamics*, 38(5-6):1031–1046, 2012.
- Maher, N. Natural Drivers of Interannual to Decadal Variations in Surface Climate. <http://handle.unsw.edu.au/1959.4/56837>, 2016. (PhD thesis retrieved from UNSW Library).
- McGregor, S., Ramesh, N., Spence, P., England, M. H., McPhaden, M. J., and Santoso, A. Meridional movement of wind anomalies during ENSO events and their role in event termination. *Geophysical Research Letters*, 40(4):749–754, 2013.
- McGregor, S., Spence, P., Schwarzkopf, F. U., England, M. H., Santoso, A., Kessler, W. S., Timmermann, A., and Böning, C. W. ENSO-driven interhemispheric Pacific mass transports. *Journal of Geophysical Research: Oceans*, 119(9):6221–6237, 2014.
- McPhaden, M. J., Zebiak, S. E., and Glantz, M. H. ENSO as an Integrating Concept in Earth Science. *Science*, 314(5806):1740–1745, 2006.
- McPhaden, M. Playing hide and seek with El Niño. *Nature Climate Change*, 2015.
- Meehl, G. A., Arblaster, J. M., Fasullo, J. T., Hu, A., and Trenberth, K. E. Model-based evidence of deep-ocean heat uptake during surface-temperature hiatus periods. *Nature Climate Change*, 1(7):360–364, 2011.
- Meinen, C. S. and McPhaden, M. J. Observations of Warm Water Volume Changes in the Equatorial Pacific and their Relationship to El Niño and La Niña. *Journal of Climate*, 13(20):3551–3559, 2000.
- Mogensen, K., Balmaseda, M. A., and Weaver, A. *The NEMOVAR ocean data assimilation system as implemented in the ECMWF ocean analysis for System 4*. European Centre for Medium-Range Weather Forecasts, 2012.
- National Oceanographic and Atmospheric Administration's Climate Prediction Center. ENSO: Recent Evolution, Current Status and Predictions. http://www.cpc.ncep.noaa.gov/products/analysis_monitoring/lanina/enso_evolution-status-fcsts-web.pdf, 2017. [Accessed: 2017-25-06].
- Nurse, L. A., McLean, R. F., Agard, J., Briguglio, L. P., Duvat-Magnan, V., Pelesikoti, N., Tompkins, E., and Webb, A. Small islands. In *Climate Change 2014: Impacts, Adaptation, and Vulnerability. Part B: Regional Aspects. Contribution of Working Group II to the Fifth Assessment Report of the Intergovernmental Panel on Climate Change* [Barros V. R., Field C. B., Dokken M. J., Mastrandrea M. D., Mach K. J., Bilir T. E., Chatterjee M., Ebi K. L., Estrada Y. O., Genova R. C., Girma B., Kissel E. S., Levy A.

- N., MacCracken S., Mastrandrea P. R. and White L.L. (eds.)]. Cambridge University Press, Cambridge, United Kingdom and New York, NY, USA., 2013.
- Roemmich, D. and Gilson, J. The global ocean imprint of ENSO. *Geophysical Research Letters*, 38(13), 2011.
- Spence, P., Griffies, S. M., England, M. H., Hogg, A. M., Saenko, O. A., and Jourdain, N. C. Rapid subsurface warming and circulation changes of Antarctic coastal waters by poleward shifting winds. *Geophysical Research Letters*, 41(13):4601–4610, 2014.
- Stewart, R. H. *Introduction to Physical Oceanography*. Texas A & M University, 2008.
- Stuecker, M. F., Jin, F.-F., Timmermann, A., and McGregor, S. Combination Mode Dynamics of the Anomalous Northwest Pacific Anticyclone. *Journal of Climate*, 28(3):1093–1111, 2015.
- Trenberth, K. E., Large, W. G., and Olson, J. G. The Mean Annual Cycle in Global Ocean Wind Stress. *Journal of Physical Oceanography*, 20(11): 1742–1760, 1990.
- Wang, Y., Gozolchiani, A., Ashkenazy, Y., and Havlin, S. Oceanic El-Niño wave dynamics and climate networks. *New Journal of Physics*, 18(3):21–33, 2016.